Vibro-Acoustic Analysis of an Underwater Cylindrical Shell with Internal Structures and a Comparison with Experiment

Lei Chen, Peng Li* and Haoran Chen

School of Mechanics and Aerospace Engineering, Applied Mechanics and Structure Safety Key Laboratory of Sichuan Province, Southwest Jiaotong University, Chengdu, 610031, P.R. China

Abstract: In this work, the low-frequency vibration response and full-band acoustic radiation characteristics of an underwater reinforced cylindrical shell with internal structures are studied by combining the FEM with SEA. The stiffened cylindrical shell contains internal structures such as the F-shape plates and the support valve frames. The exciting sources have two different exciting forces corresponding to two experimental conditions. In the low-frequency band, the FEM was employed, and in the medium and high-frequency bands, the SEA was used. A comparison of the numerical results and the experiment shows that they agree well. The FEM and SEA give better results at [1,1k] Hz and [1k,10k] Hz, respectively. Due to mesh quality limitations, the FEM is not favorable for medium and high-frequency calculations. The SEA focuses on the structural mean power flow but cannot obtain position-specific vibrational responses. The results show that the internal excitation source mainly causes the structural vibration and sound radiation and are closely related to the free vibration characteristics of the structure. In addition, with the increase in frequency, the circumferential sound pressure level of the underwater structure has more substantial directivity.

Keywords: FEM, SEA, Stiffened cylindrical shell, Full band, Vibration, Acoustic.

1. INTRODUCTION

The excitation load of internal mechanical equipment in a structure like an underwater vehicle will harm the structure, leading to complex wide-band vibration and sound radiation that will damage the structure function and jeopardize the staff's health. Underwater vehicles, like a submarine, mainly comprise cylindrical shells, ring ribs, seal plates, and complex internal structures. The annular reinforced cylindrical shell is a typical structure in the aviation or shipbuilding industry. In fluid-structure coupling dynamics, the vibration and sound radiation of the reinforced cylindrical shell submerged in water are a classical problem of FSI field. Studying underwater vibration and acoustic radiation properties of stiffened cylindrical shells with complex structures is vital for vibration and noise control of underwater vehicles.

Currently, there are numerous theoretical approaches to the dynamic properties of shells [1], such as wave propagation method [2], transfer matrix [3], energy [4]. In addition, many scholars have also studied the acoustic and vibration response of shell structures. Polyakov *et al*. [5] studied the finite solution of the radius wave problem for closed spherical shells with different thicknesses by using the method of separation of variables. Hodges *et al*. [6, 7] established a cylindrical shell model with a T-shape fin and calculated the vibration characteristics of the cylindrical shell in the low-frequency band based on the energy method, which are in good agreement with the experimental results. Photiadis *et al*. [8] analyzed the influence of structural resonance on structural acoustic properties, including curved Bloch mode resonance and local resonance caused by irregular structure. Based on the mode decomposition technology, the structure's vibration response and acoustic radiation under the action of propeller forces were calculated. The validity of the numerical results were verified by comparison with the theoretical, literature and experimental results. Li *et al*. [9] established a nonlinear response test system for cylindrical shells and conducted in-depth experimental research on the nonlinear vibration of thin-walled cylindrical shells under point support conditions. Wang *et al*. [10] studied the free vibration of hyperbolic rotating shell structures under arbitrary boundary conditions by using the Jacobi-Ritz formula, established a theoretical model by using multi-segment division and Flugge thin shell theory, and simulated arbitrary boundary conditions as well as motion compatibility and physical compatibility conditions at the interface by using boundary and coupled spring techniques. Qin *et al*. [11] studied the free vibration characteristics of a single cylindrical shell under arbitrary boundary conditions based on Sanders shell theory and the establishment of artificial springs at both ends of the shell and discussed different expansion forms of shell displacement. Chebyshev polynomial has higher computational efficiency.

*Address correspondence to this author at the School of Mechanics and Aerospace Engineering, Applied Mechanics and Structure Safety Key Laboratory of Sichuan Province, Southwest Jiaotong University, Chengdu, 610031, P.R. China; E-mail: meiyongyuandeze@163.com; lp_vib@126.com

E-ISSN: 2409-9848/23

Some scholars also focus on the solution of sound radiation. Guo *et al*. [12] uses the analytical and boundary element coupling method to solve the acoustic radiation of a single cylindrical shell at a finite depth from the free liquid surface. The shell vibration is described based on the Flugge and Laplace equations, and the boundary element method solves the far-field acoustic radiation. Aslani *et al*. [13] gives a radiation mode of an external radiating cylinder that considers axial and circumferential dependence, more naturally matching the geometry. Caresta [14] used the wave propagation method and the power series method to study the specific response of the submarine model with a conical shell at both ends and a cylindrical shell in the middle. The sound field solution was based on the Helmholtz integral. Wang and their colleagues [15-18] have conducted extensive studies on the vibration response of single-shell structures and coupled shell structures, extended the exact transfer matrix method (PTMM), calculated the vibration response and sound radiation of ring-rib cylindrical shells under light and heavy fluids within [1,3k] Hz, and studied the relationship between the peak sound pressure and the natural frequency of the structure. Based on the energy method, Jin *et al*. [19] studied the external response and acoustic radiation of a cone-cylindrical-hemispherical coupled shell with bulkhead and ring ribs in a heavy fluid and verifies the effectiveness of the proposed method by comparing it with the finite element results.

In addition, several researchers have examined the shell's vibration properties and acoustic radiation using the finite element method and experiment. Yildizdag *et al*. [20] researched the vibration response and sound radiation of a largely water-filled cylindrical shell by using the coupling approach of finite element and boundary element, which is based on the Love shell theory and is in good accord with the experimental data. Gao *et al*. [21] experimented on the stiffened cylindrical shell's acoustic radiation and vibration response at [1,2.5] kHz. Mechanical forces are primarily responsible for the structure's high-frequency vibration response and sound radiation. Li and Hua *et al*. [22, 23] developed the "propeller-shafting-hull" complicated coupling system model by utilizing the boundary element and finite element coupling methods. Maxit and Ginoux *et al*. [24-26] established a numerical model of the sound scattering of a non-equidistant stiffened cylindrical shell with water attached using the circumferential admittance method (CAA). The internal frame and shell were separated into various subsystems, and experiments were used to confirm that the numerical model was accurate. Chen *et al*. [27] put out a hybrid analytical-numerical approach to address the vibration characteristics of a cylindrical shell with interior structure. The finite element approach was used to describe the internal structure, the wave function was used to define the shell motion equation, and an artificial spring was used to precisely simulate the boundary conditions at the point where the internal structure and shell joined. Yi *et al*. [28] studied the flow-induced structural noise of submerged cone-cylindrical hemisphere shell under turbulent excitation and conducted experiments in a low-noise gravity water tunnel based on the mixed algorithm of computational fluid dynamics (CFD) and computational acoustics (CA). The results of the simulation and the experiment agree fairly well. Gupta [29] introduced non-harmonic stimulation in addition to harmonic excitation and used statistical energy analysis to investigate the transmission loss of cylindrical acoustic enclosures in various frequency zones. The computation of high-frequency transmission can be done by using the statistical energy anslysis approach.

As previously noted, numerous theoretical, computational, and experimental investigations have been conducted regarding the acoustic and vibration properties of single-shell, coupled-shell, double-shell, and reinforced-shell structures. Nevertheless, the following are the studies' shortcomings: Firstly, the research methods related to vibration characteristics and sound radiation are more theoretical than numerical simulation and experiment. As a result, the complex structure inside the cylindrical shell, such as ring ribs, sealing plate, internal valve frame, F-shape plates and exciters, will be ignored when solving, which is quite different from the actual engineering model. In addition, the researchers usually assume that only one part of the cylindrical shell is stimulated, which is different from the multi-device excitation of the actual underwater vehicle operation. Secondly, the frequency range chosen by some researchers is limited, and it is difficult to calculate the full-band acoustic and vibration characteristics of complex cylindrical shells. On the one hand, due to the problem of computational efficiency, structural sound radiation at high-frequency band may require more computer resources; on the other hand, due to the limitations of theoretical methods, the calculation process may be difficult to converge at high frequency, and there is no good accuracy. Finally, the relationship between the acoustic and vibration characteristics of the reinforced cylindrical shell with

complex structure underwater and the internal exciting force and its own vibration characteristics, as well as the axial and circumferential distribution of the sound pressure level of the cylindrical shell structure is also a problem worth exploring. This study establishes a FE model and a SEA model of an underwater stiffened cylindrical shell with a complex internal structure by combining various acoustic calculation methods. The vibration response and sound pressure level of the cylindrical shell under the action of multiple mechanical equipment and full-frequency excitation loads are calculated to establish the full-frequency noise analysis. The suggested method's accuracy is confirmed by comparison with the experiment.

2. MODEL DESCRIPTION

2.1. Numerical Model

An underwater reinforced complex cylindrical shell should have vibration and sound radiation analysis considering the fluid-structure coupling effect. This paper utilizes the general finite element coupling method and statistical energy analysis method, which give a reasonable calculation frequency bandwidth allocation, avoid the middle and high-frequency bands grid problem, reduce the solution dimension, and increase calculation efficiency.

2.1.1. Equation of Acoustic-Solid Coupling FEM

The finite element vibration equation of the structure can be give by [21]:

$$[M_S]\{\ddot{x}(t)\}+[C_S]\{\dot{x}(t)\}+[K_S]\{x(t)\}=\{F_S\} \tag{1}$$

To deal with the coupling between solid structure and fluid sound field, commercial software ANSYS provides Fluid30 elements to simulate fluid medium and Fluid130 elements the sound absorption boundary. Assuming fluid is compressible, irrotational, and without body force and mean flow. The Fluid 30 elements use the N-S equation as the governing equation of the fluid. The matrix form of the discrete acoustic wave equation can be derived as:

$$[M_F]\{\ddot{p}_e\}+[C_F]\{\dot{p}_e\}+[K_F]\{p_e\}+\overline{\rho}_0[B]^T[\ddot{x}(t)]=\{F_F\} \tag{2}$$

Let $\{F^{pr}\}$ be the fluid force acting on the interaction surface must be considered to describe the FSI problem, then, Eq.(1) can be written as:

$$[M_S]\{\ddot{x}(t)\}+[C_S]\{\dot{x}(t)\}+[K_S]\{x(t)\}=\{F_S\}+\{F^{pr}\} \tag{3}$$

where

$$\{F^{pr}\}=[B]\{p_e\} \tag{4}$$

By combining Eqs.(2), (3) and (4), the complete sound-structure coupling equation can be obtained by combining the equations as follows [31]:

$$\begin{bmatrix}[M_S] & 0\\ \overline{\rho}_0[B]^T & [M_F]\end{bmatrix}\begin{Bmatrix}\{\ddot{x}(t)\}\\ \{\ddot{p}_e\}\end{Bmatrix}+\begin{bmatrix}[C_S] & 0\\ 0 & [C_F]\end{bmatrix}\begin{Bmatrix}\{\dot{x}(t)\}\\ \{\dot{p}_e\}\end{Bmatrix}+\begin{bmatrix}[K_S] & -[B]\\ 0 & [K_F]\end{bmatrix}\begin{Bmatrix}\{x(t)\}\\ \{p_e\}\end{Bmatrix}=\begin{Bmatrix}\{F_S\}\\ \{F_F\}\end{Bmatrix} \tag{5}$$

The harmonic response analysis in ANSYS can solve the finite element discrete equation of the whole system, so as to obtain the concrete vibration response of the structure and the sound pressure distribution of the flow field.

2.1.2. Basic Description of SEA

The SEA approach is helpful for researching how randomly excited complex structures at medium and high frequencies respond to sound. It studies the energy transmission and balance between systems using statistical notions and analyzes the coupling dynamics of high frequency and high modal density complex systems. It can break down a complicated system into many easily understood subsystems. In the SEA, energy is employed as an independent dynamic variable to address the coupling dynamics between solid structure and fluid sound field. Power flow is used to characterize the interaction between coupling subsystems. Energy is also used to define the state of each subsystem. The limitation and characteristic of the SEA method is that, while it cannot precisely anticipate the response of a given local place within the subsystem, it can more accurately predict the overall response level of the subsystem based on a statistical sense. The energy transfer between the two subsystems can be described as [30, 32]:

$$P_{i,in}=\omega\sum_{k=1}^{n}\eta_{ik}E_i+\omega\sum_{j=1,j\neq i}^{n}\eta_{ji}E_j \tag{6}$$

It is possible to calculate the system's statistical energy characteristics as well as the energy of each subsystem within the frequency range. After that, the dynamic response, including the sound pressure level and vibration velocity, can be obtained. This work establishes the SEA model and computes the sound pressure level by using the commercial software VAOne.

2.2. FE and SEA Models of the Experimental Model

As shown in Figure **1**, the experimental model is a stiffened cylindrical shell with some complex internal structures. Its interior contains two F-shape plates, an I-beam support valve frame, some ring ribs, two motors, a front sealing plate and a back sealing plate. The F-shape plates, ring ribs, and the cylindrical shell are welded together. Twelve isolation springs connect the F-shape plates to the support valve frame. The two motors on the support valve frame numbered 1 and 2, serve as the excitation source. Four steel rods link each motor to the support valve frame, and the exciting force generated by the motor is F_1 and F_2, respectively. Above the support valve frame is where many counterweights are welded. A sealing plate seals the cylindrical shell's two ends, and the sealing plate and shell are joined by welding. The front and rear sealing plates are equipped with several elbow plates. The reinforced cylindrical shell is axisymmetric. Table **1** displays the cylindrical shell model's material and physical characteristics.

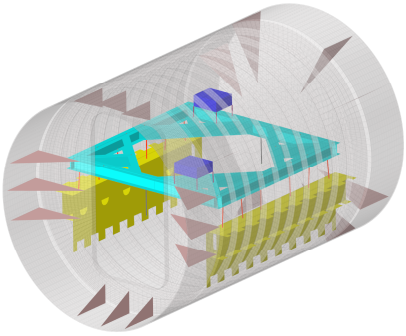

(a) 3D schematic diagram of the experimental model of the structure

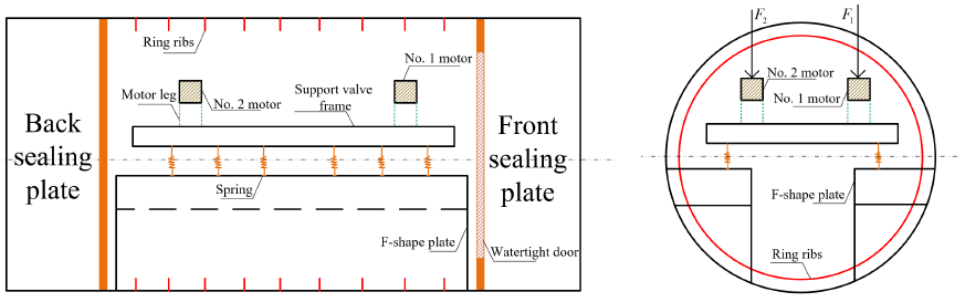

(b) Front view **(c)** Left-side view

Figure 1: Schematic diagram of the experimental model.

Table 1: Dimensions of the Shell and Internal Structure

Parameters	Value	Parameters	Value
Total length	3 m	Number of ring ribs	9
Radius	1.017 m	Thickness of ring ribs	0.008 m
Cylindrical shell thickness	0.008 m	Height of ring ribs	0.07 m
Sealing plate thickness	0.056 m	Support valve frame thickness	0.005 m
Modulus of elasticity	206 GPa	F-shape plates thickness	0.01 m
Poisson's ratio	0.3	Tail length of the shell	0.495 m
Length of shell with ring rib	2 m	Head length of the shell	0.505 m
Quality	8547 kg	Density	7850 kg/m^3

Table 2: Introduction of the Elements Required when Building the FE Model

Elements	Introduction
SOLSH190	3D 8-Node structural solid shell element
SHELL181	4-Node structural shell element
COMBIN14	Spring damping element
BEAM188	3D 2-Node beam element
FLUID30	3D 8-Node acoustic fluid element
FLUID130	3D Infinite acoustic

Figures **2** and **3** display the FE and SEA models depicted in Figure **1**. The description of the elements required for FE models is shown in Table **2**. SOLSH190 elements are applied to build the cylindrical shell and ring ribs, and SHELL181 elements are used to build the internal support valve frame and F-shape plate. The twelve springs that attach the F-shape plate to the support valve frame are constructed with COMBIN14 elements. The cylindrical shell and F-shape plate are connected by using the MPC method. The motor legs, constructed with BEAM188 elements, and the motors with SOLSH190 elements connect the two motors to the support valve frame. The motors, motor legs, and support valve frame are connected through common nodes. The external shell of the experimental model shown in Figure **1** is used as an example. It is calculated that when the radius of the outer water area is more than 2.5 times the radius of the cylindrical shell, the influence of the water area size on the frequency of the cylindrical shell can be negligible. Therefore, the radius of the water area in this work is three times that of the shell. FLUID30 elements are used to establish the external water area, and FLUID130 elements are used to establish the sound absorption boundary to simulate the infinite water area.

The modal density in the analysis bandwidth (f_a) is less than 1, Figure **3**(**b**) [32], demonstrating that the low-frequency range of [1,1k] Hz is the reason for the sparse modes of the cylindrical shell. The FE model is utilized for calculations in this low-frequency band. In the range of [1,315] Hz, the calculated frequency interval (Δf) is 1 Hz due to the exciting force changes dramatically. In the range of [315,500] Hz, Δf =5 Hz. In the range of [500,1k] Hz, Δf =10 Hz. The SEA model was used in medium and high-frequency bands. The value ranges are [1k,10k] Hz, Δf =10 Hz. In the FE model, in order to effectively ensure calculation accuracy and solution efficiency, the relationship between the maximum mesh size and the minimum bending wavelength in the medium can be determined by:

$$L_{\max} \le \lambda_{\min} / 6 \tag{7}$$

$\lambda_{\min}$ is defined as follows:

$$\lambda_{\min} = \sqrt{\frac{2\pi}{f_{\max}}} \sqrt[4]{\frac{Eh^2}{12\rho(1-\mu^2)^2}} \tag{8}$$

In the FE model, $f_{\max}$ =1k Hz [21].

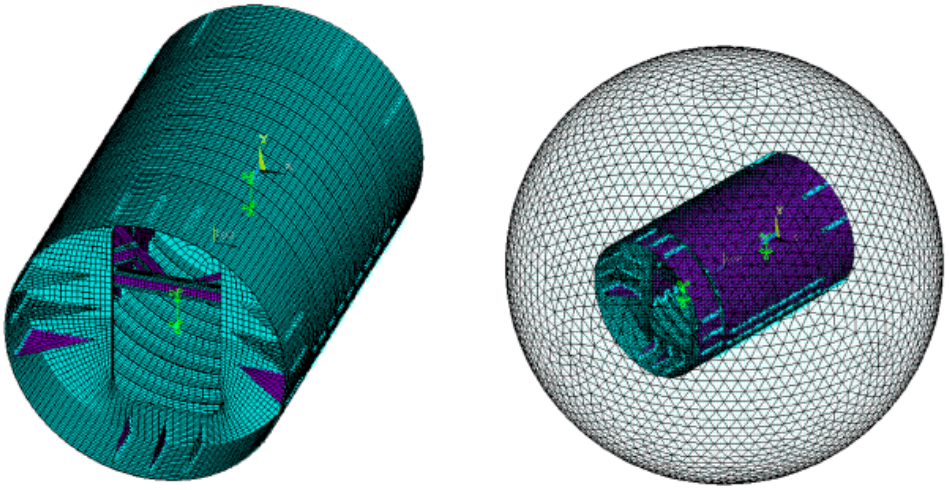

(a) Structural FE model

(b) FE model of the water-attach structure

Figure 2: FE model for low-frequency calculation.

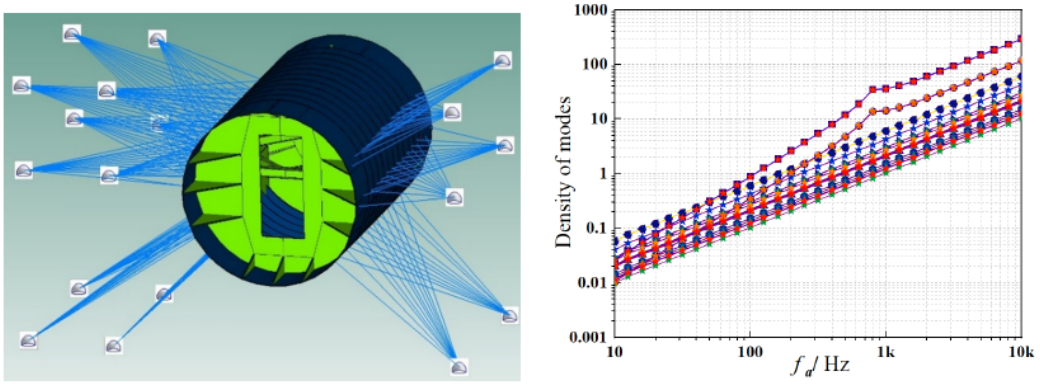

(a) Structural SEA model **(b)** Substructure modal density

Figure 3: Medium and high-frequency bands SEA models and modal density.

Considering that the upper limit of the low-frequency calculation frequency in our present study is 1k Hz, the thickness of the cylindrical shell is 0.008 m, and the maximum mesh size is 0.048 m, the mesh size of the structure in FE model is set as 0.045 m, which can meet the requirements of calculation accuracy. And the total numbers of structure meshes are 35293. At the highest computed frequency, the fluid grid must be less than one-tenth of the sound wave wavelength in the acoustic medium. Since sound waves in water have a wavelength of 1.5 meters, fluid mesh sizes cannot be larger than 0.15 meters, and there are 193440 fluid meshes.

3. EXPERIMENTAL SETUP

3.1. Experimental Test Site Layout

Figures **4**(**a**, **b**) depict the structural vibration response measuring points, and 18 points are set. The measuring points are arranged in axial and

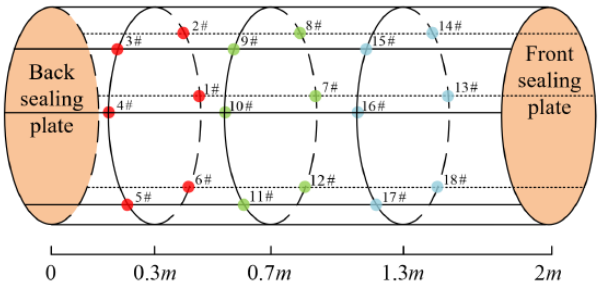

(a) Overall diagram of structural vibration response measuring points

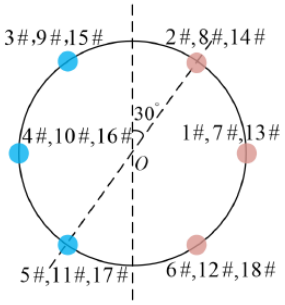

(b) Side view of structural vibration response measuring points

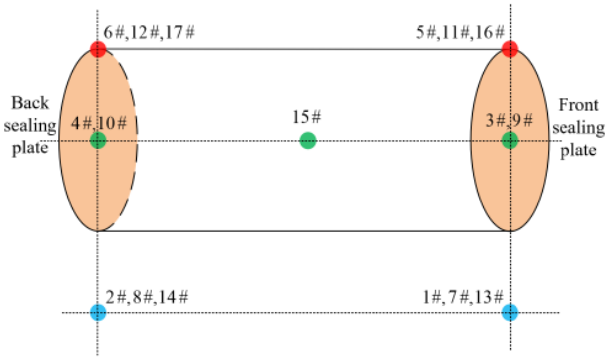

(c) Overall diagram of structural sound pressure level measuring points

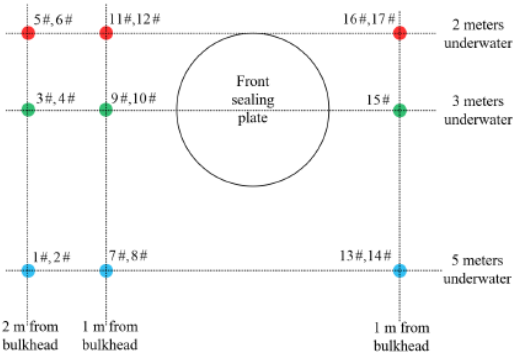

(d) Side view of structural sound pressure level measuring points

Figure 4: Structural vibration response and sound pressure level measuring points diagram.

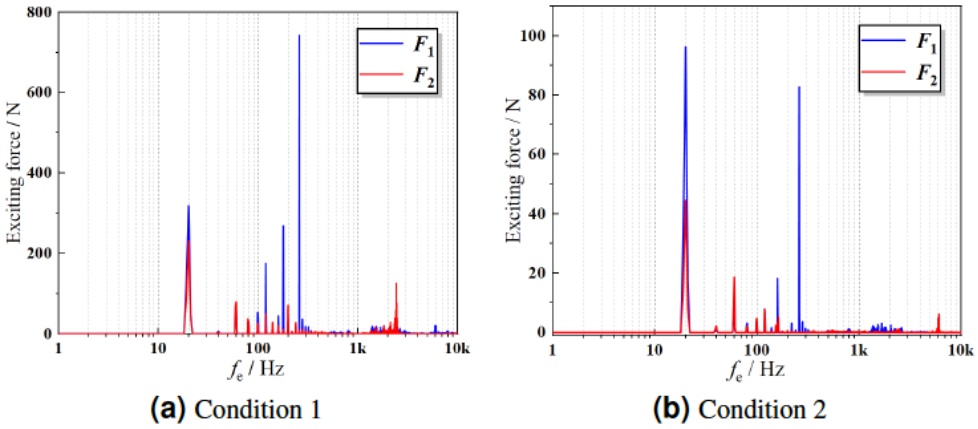

Figure 5: Exciting force of two motors under different working conditions.

circumferential directions. It is used to measure the radial acceleration of the shell surface. The distances between the measuring points and the back sealing plate are 0.3, 0.7, and 1.3 meters, respectively. Figures **4**(**c**, **d**) display the sound pressure level measuring points, and 17 points are set. They are arranged at 2, 3 and 5 meters underwater, and 1 and 2 meters away from the cylindrical shell bulkhead. Measuring points cover the front, middle and rear sections of the structure. It is used to measure the radiation noise of the structure in water.

3.2. Excitation Force Load

As shown in Figure **5**, the working conditions under the influence of two distinct excitation forces are analyzed in this study. Under the two working conditions, the FE-SEA method calculates the structural vibration response in the low-frequency band and the sound pressure level in the full-frequency band. The first condition is a high-power operation of the motor, and the second condition is a low-power operation. Figure **5** shows the excitation forces of F_1 and F_2 of the two different motors at the working conditions 1 and 2. The excitation frequency (f_e) range is [1,10k] Hz.

4. RESULTS, COMPARISON AND DISCUSSION

4.1. Free Vibration Analysis

The cylindrical shell vibration and sound radiation dispersion are correlated with its frequency and mode. Figure **6** shows the frequency and mode diagram of the

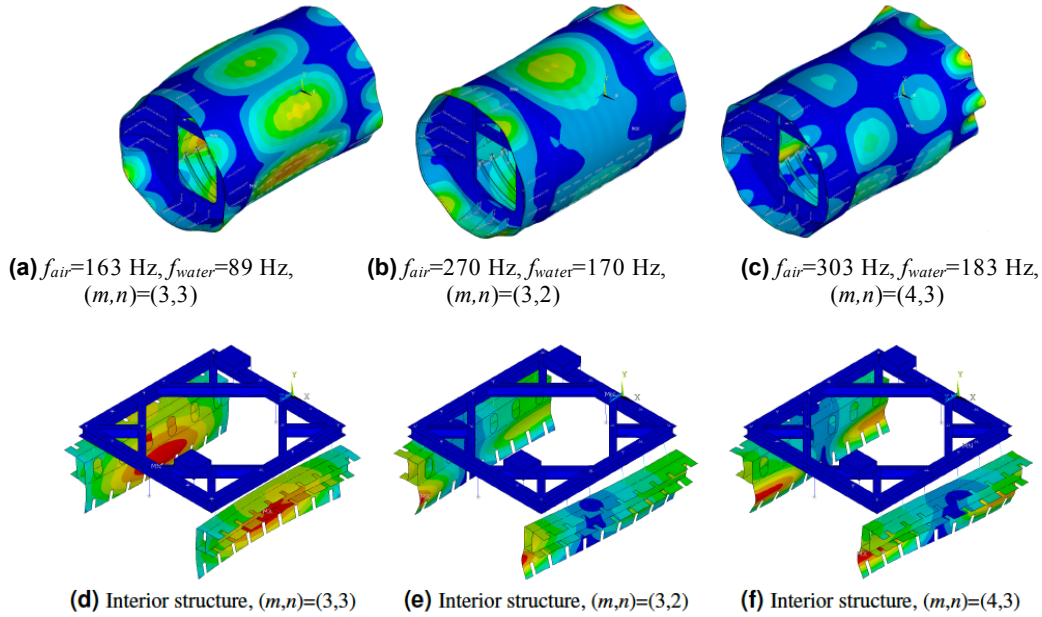

Figure 6: Frequency and mode of the structure in air and water (m and n represent axial and circumferential wave numbers respectively).

stiffened cylindrical shell and its interior structure in air and water. It can be seen from the figure that the frequency in water (f_{water}) is significantly lower than that in air (f_{air}). In addition, due to the action of reinforcement, the circumferential stiffness of the srutcture is enhanced. The cylindrical shell cannot easily appear in circumferential mode, and axial mode is more likely to appear. Because the F-shape plates are directly related to the shell, the deformation of the internal structures are also mainly concentrated at the F-shape plates.

4.2. Forced Vibration Analysis and Experiment Comparison

The low-frequency band calculating frequency (f) range is [1,1k] Hz, as can be seen from the results above. A comparison between the vibration response measured by FEM and the experiment is presented in Figure **7**, which shows the vibration response at various places within the structure. Vibration acceleration level is calculated from the experimental and FEM data by:

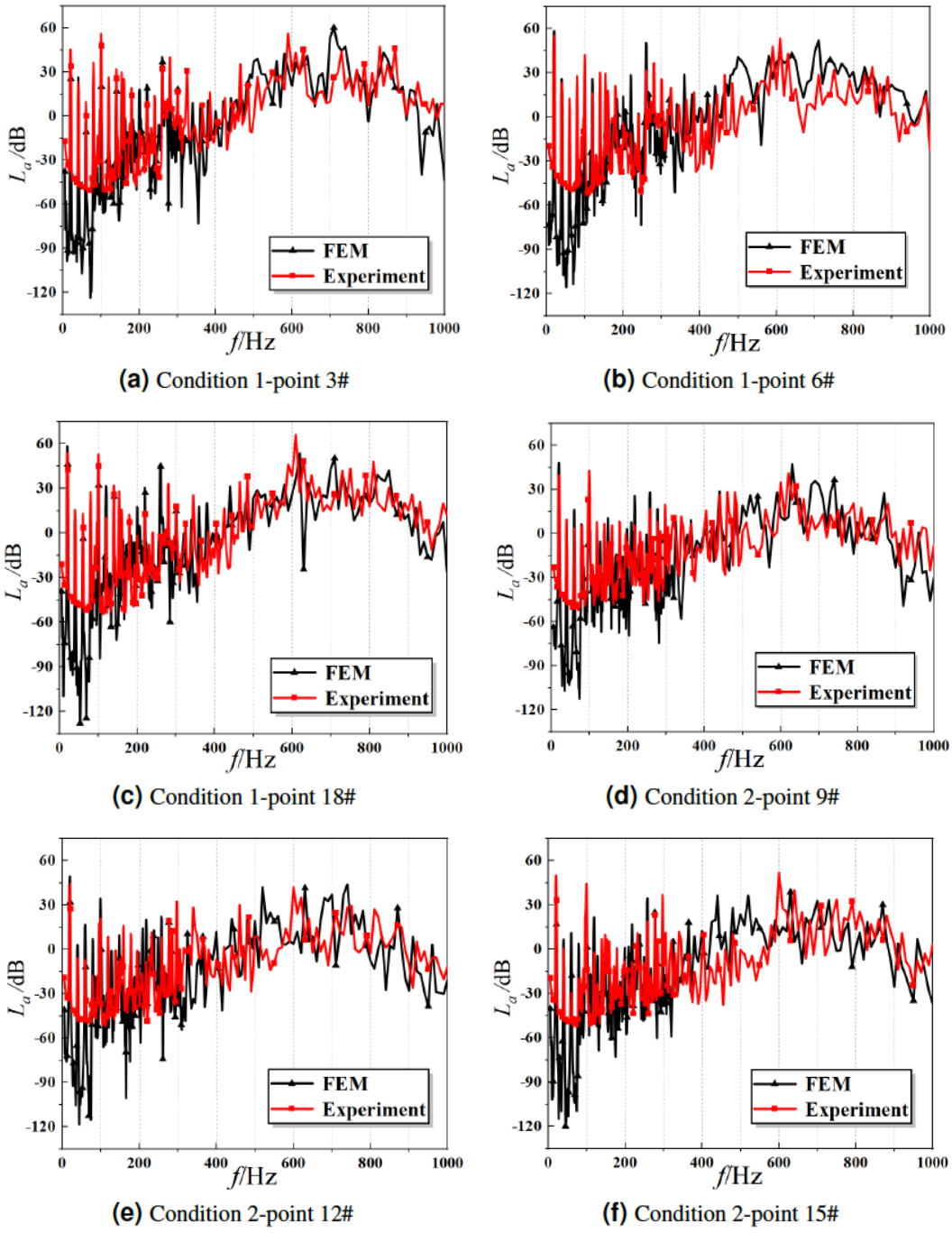

Figure 7: Low-frequency vibration acceleration level at different measuring points under different working conditions.

$$\begin{cases} L_a = 20 * \lg(a / a_0) \\ L_p = 20 * \lg(p / p_0) \end{cases} \quad (9)$$

The FEM results and experimental vibration acceleration levels are displayed in Figure **7**. The three measuring points of working condition 1 are shown in Figures **7**(**a**, **b**, **c**); the three measuring points of working condition 2 are shown in Figures **7**(**d**, **e**, **f**). The two results show good agreement in the [1,1k] Hz range. There are some discrepancies between the results of the FEM calculation and the experiments when $f < 315$ Hz. The primary cause of the problem is that the motor generates extra mass effects, which are more noticeable at low frequencies. The extra mass of the motor is not sufficiently represented in the FEM [21]. In addition, the fact that the experimental conditions cannot satisfy the infinite water in the FE model is also one of the influencing factors, like finite depth from the free surface [12, 22].

4.3. Acoustic radiation analysis and experiment comparison

This section analyses the structureal sound pressure level at the full-frequency band, and the calculating frequency (f) falls between [1,10k] Hz. Two measuring points at 3 m and 5 m underwater were selected to calculate the sound pressure level. Figure **8** compares the experimental sound pressure level results with the FEM results. The f is in the [1,1k] Hz range. The data calculated by the experiment and FEM were converted into sound pressure levels according to Eq.(9). Figure **8** shows the FEM results and experimental sound pressure levels. The FEM results show good agreement with experiments in the [315,1k] Hz. When $f < 315$ Hz, there are errors between FEM calculation results and experiments. The main reasons for this phenomenon are as follows: Firstly, the FEM does not entirely account for the additional mass effect that the motor produces, which is particularly noticeable in low-frequency band. Additionally, there will be some sound wave reflection in the low-frequency band because of these waves' longer wavelength and higher energy. However, the sound absorption equipments of test site make it difficult to eradicate this reflection [18, 21, 33].

According to Figures **7** and **8**, when f is 89 Hz, 170 Hz and 183 Hz, under two working conditions, the

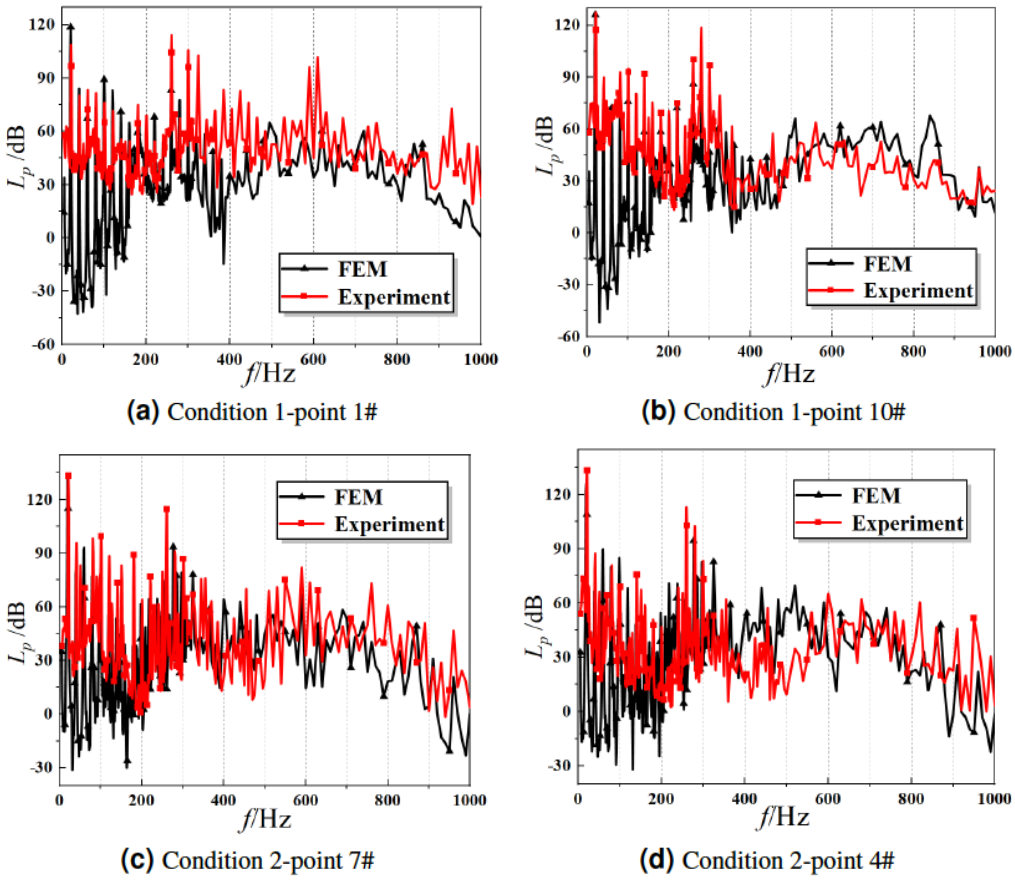

Figure 8: Low-frequency bands sound pressure levels at different measuring points under different working conditions.

structural vibration response and sound pressure level appear to be extreme levels. The structureal peak sound pressure level and vibration response correlate with the structureal free vibration frequency in water when the motor is stimulated.

Figure **9** displays a comparison of the experimental sound pressure level and the SEA. The f band is [1k,10k] Hz. The comparison of the experimental and SEA results reveal that in the [1k,10k] Hz frequency range, the variation trend of the sound pressure level curve calculated by SEA is in good agreement with the experimental results, and the extreme value appears near 6k Hz.

To sum up, the sound pressure level calculation results of FE and SEA are integrated, as shown in Figure **10**. The low-frequency range is [1,1k] Hz, and the medium and high-frequency range is [1, 10k] Hz. The results of measuring points 1# and 10# in the working condition 1 and 4# and 7# in the working condition 2 can be obtained. The calculated results of FE-SEA method are in good agreement with the experimental results.

The results of Figure **10** show that the sound pressure level fluctuates sharply in the low and middle-frequency bands of [1,2k] Hz. The sound pressure level is low and relatively stable in the middle and high-frequency bands of [3k,5k] Hz and [7k,10k] Hz. The sound pressure level fluctuates significantly in the high-frequency band of [5k,7k] Hz. Combined with Figure **5**, it can be seen that the sound pressure level fluctuates wildly when the motor excitation force peaks, showing that the sound radiation of the cylindrical shell structure is closely related to its internal excitation force [18, 21, 28].

4.4. Vibration Response and Acoustic Radiation Characters

The comparison between the previous and experimental results demonstrates the accuracy of the

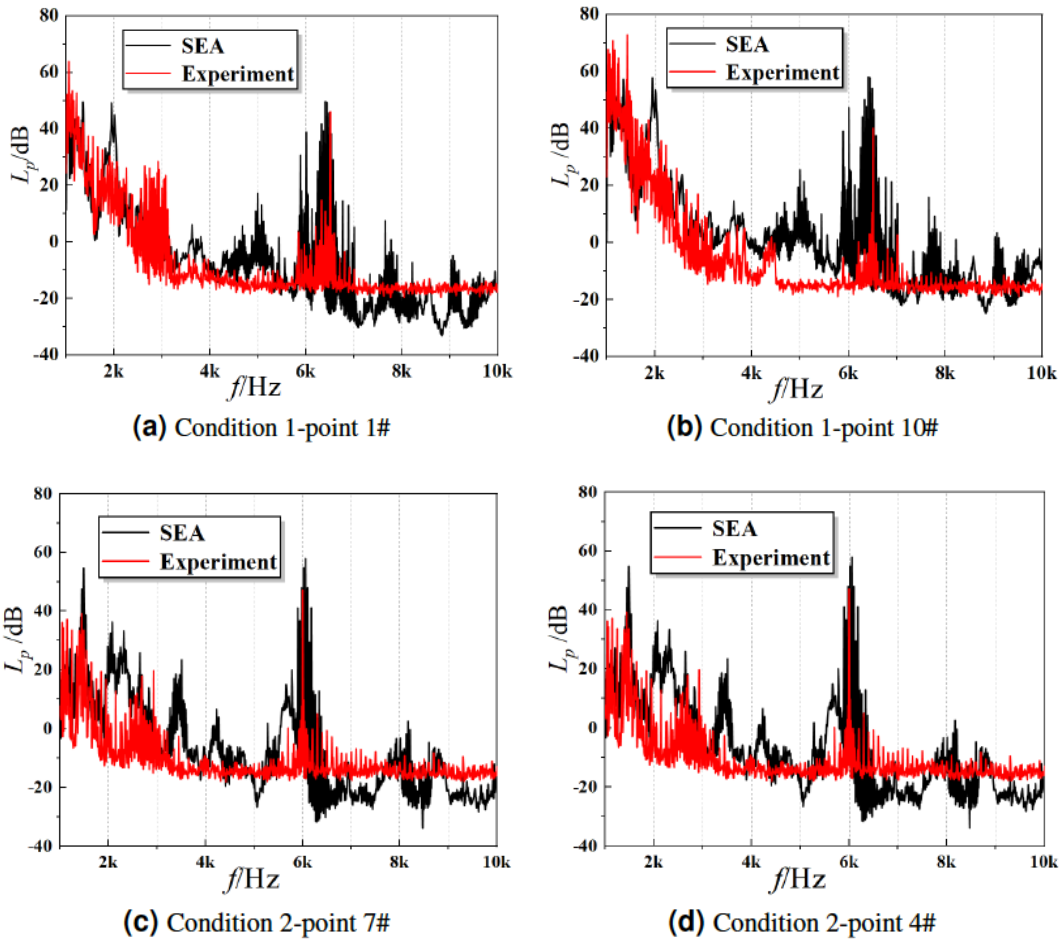

Figure 9: Medium and high-frequency bands sound pressure levels at different measuring points under different working conditions.

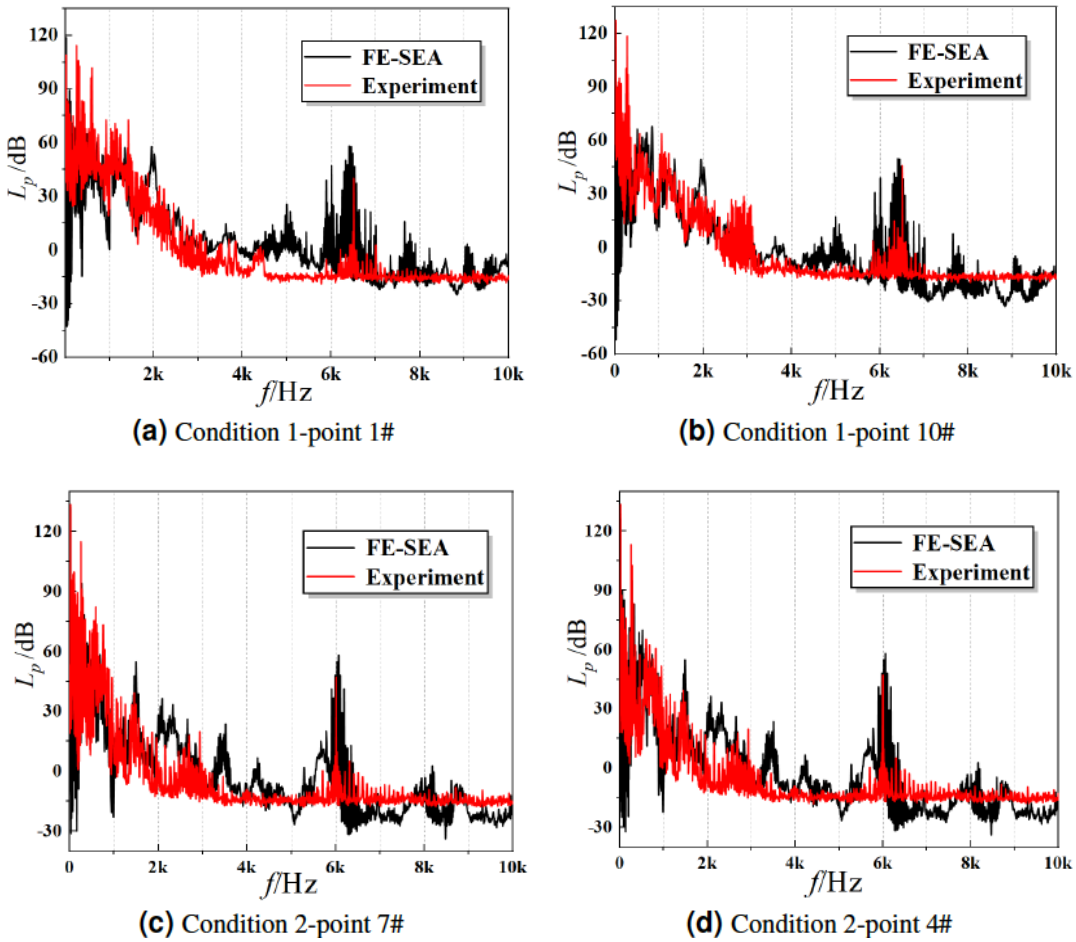

Figure 10: Full-band sound pressure levels at different measuring points under different working conditions.

numerical model and the method used in this article. In order to gain a more comprehensive understanding of the vibration and sound radiation characteristics, we will now examine the distribution characteristics of shell vibration response and sound pressure level on the shell surface.

Figures **11** (**a**, **b**) show the vibration acceleration levels of different measuring points under the same angle of the structure in condition 1 at the low-frequency band (f ＜1k Hz). Figures **11** (**c**, **d**) show the vibration acceleration levels of different measuring points under the same cross-section of the structure in condition 1 at the low-frequency band. Table **3** shows the total vibration acceleration level of differrnt measuring points of the structure in condition 1 at the low-frequency band. It can be seen that the trend and value of vibration acceleration level at different measuring points are similar at the same angle. However, measuring points 13# and 18# fluctuate more dramatically because they are closer to the excitation sources (motor 1 and motor 2). In the same section, the vibration acceleration level of different measuring points are relatively similar. However, the vibration acceleration level of measuring points 2# and 14# are significantly larger than that of other measuring points because they are closer to the position of the excitation sources (motor 1 and motor 2).

Synthesize the total vibration acceleration levels of Figure **11** and Table **3**. It can be seen that since measuring points 1#, 7#, and 13# are at the same angle, and their combined distance from motor 1 and motor 2 is similar, their total vibration acceleration levels are also similar. Measuring points 13#, 14#, and 18# are in the same section and close to motor 1, so it can be considered that the exciting force generated by motor 1 is dominant. It is obtained that the total vibration acceleration level of measuring point 14#, which is closest to motor 1, is also the highest. At the same time, this phenomenon is closely related to the vertical direction of the exciting force on the two motors.

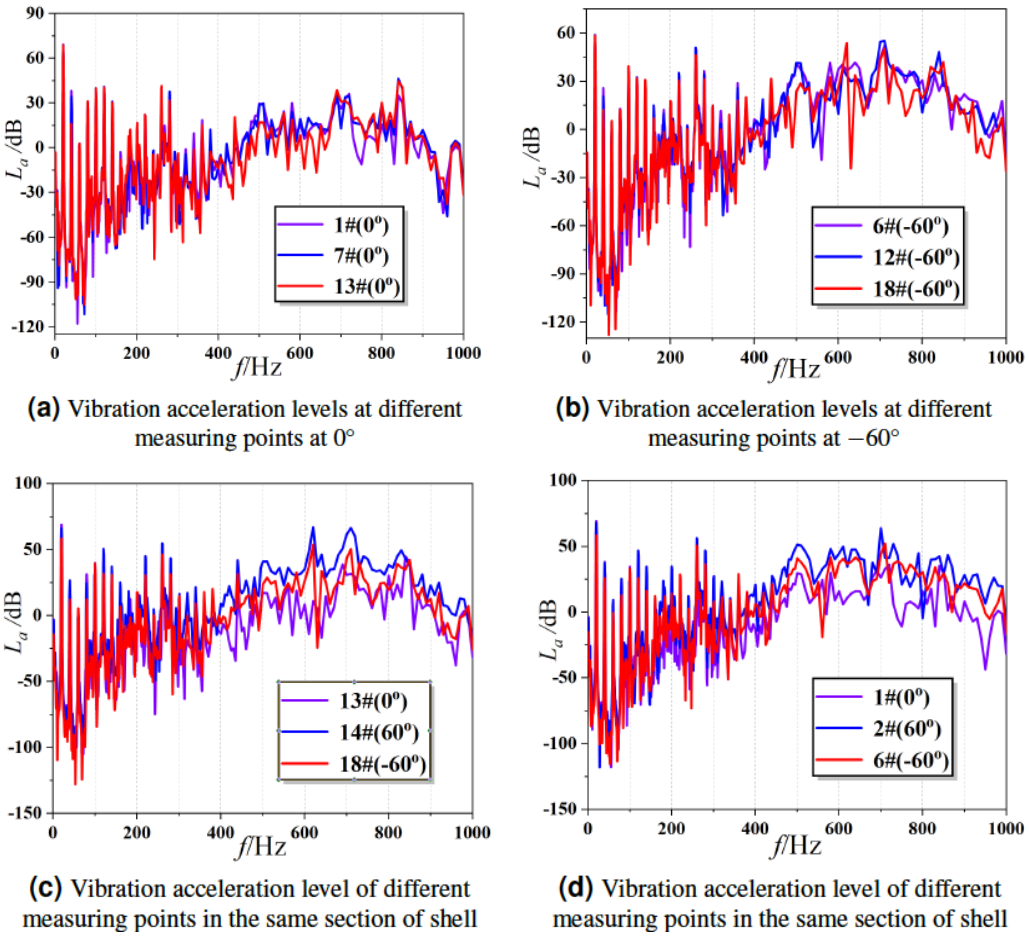

(a) Vibration acceleration levels at different measuring points at 0°

(b) Vibration acceleration levels at different measuring points at −60°

(c) Vibration acceleration level of different measuring points in the same section of shell

(d) Vibration acceleration level of different measuring points in the same section of shell

Figure 11: Vibration acceleration level of measuring points at different positions of shell surface at condition 1.

Table 3: The Total Vibration Acceleration Level of Different Measuring Points

Points	1#	2#	6#	7#	12#	13#	14#	18#
Total vibration acceleration level/dB	69.67	70.41	60.96	69.64	62.68	69.41	72.43	61.01

Figure **12** shows the comparison between the FE-SEA method and the experimental total sound pressure level. In combination with Figures **8**, **9** and **10**, although the peaks of FE-SEA and experimental formant are slightly different in some frequency bands, the total sound pressure level of the two are basically consistent. The total sound pressure level is close to the maximum value of the whole band sound pressure level. Figure **12** further proves the accuracy of FE-SEA method in calculating full-band acoustic radiation.

The distribution diagram of the sound pressure level measuring points around the structure are shown in Figure **13**. There are two circles, one in the middle and the other in the top portion (front sealing plate) of the structure, each with a total of thirty points, and the points circle the structure and distance from the bulkhead at one meter. Measuring points that are arranged are chosen for analysis.

Figure **14** shows the structural circumferential sound pressure level distribution curve, which was produced using the FEM. Figure **15** shows the cloud image of sound pressure distribution of the structure under force excitation when the measuring points are located at the top. Three frequencies with more obvious excitation force were taken for analysis. As can be seen from Figures **14** and **15**, in the low-frequency range (f < 1k Hz), The structure sound pressure level is mainly concentrated near 90° and 270°, closely correlating with the structure excitation position and direction, for example, at 20 Hz. With the increase in frequency, the sound pressure level distribution no longer has apparent symmetry but has more obvious

directivity, and the sound pressure distribution gradually becomes dense and concentrated, for example, at 800 Hz. With the change of the position of the measuring points, the sound pressure level at the top is lower than that at the middle position, and the circumferential sound pressure level curves corresponding to 260 Hz and 800 Hz have apparent changes. However, the difference at 20 Hz is only numerical data, the change of circumferential sound pressure level curve is not obvious.

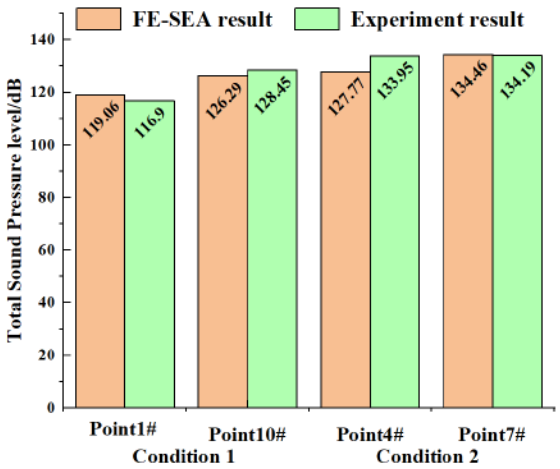

Figure 12: Comparison of total sound pressure levels in all frequency bands at different conditions.

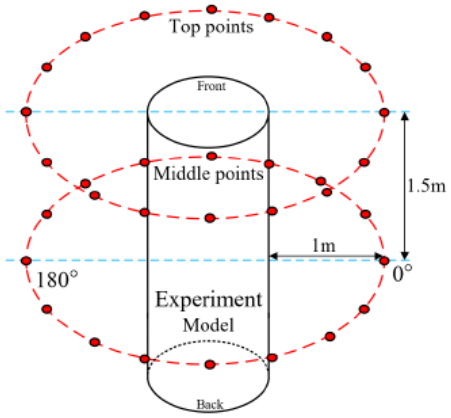

Figure 13: Circumferential distribution of sound pressure level measuring points of the structure.

Figure **16** shows the sound pressure level curve at 1/3 frequency times calculated using the SEA method. Four measuring points at different positions were selected for analysis. It can be seen that the overall trend of sound pressure level at different measuring points is consistent. In the case of the same section in the middle or top, the sound pressure level value is the same. At the same angle, the sound pressure level at the top is smaller than that in the middle, inseparable from the SEA method's statistical principle.

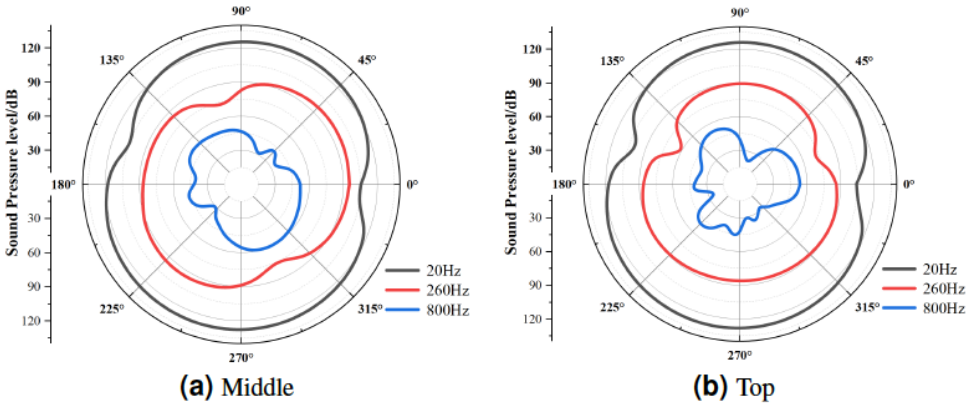

Figure 14: Circumferential sound pressure level distribution of the structure.

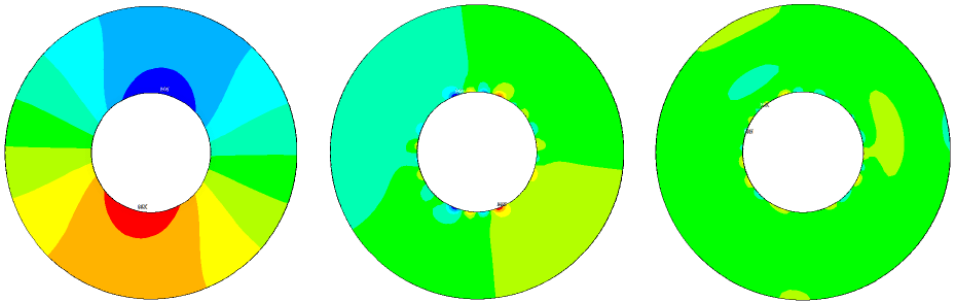

Figure 15: Cloud map distribution of sound pressure around the structure [Top].

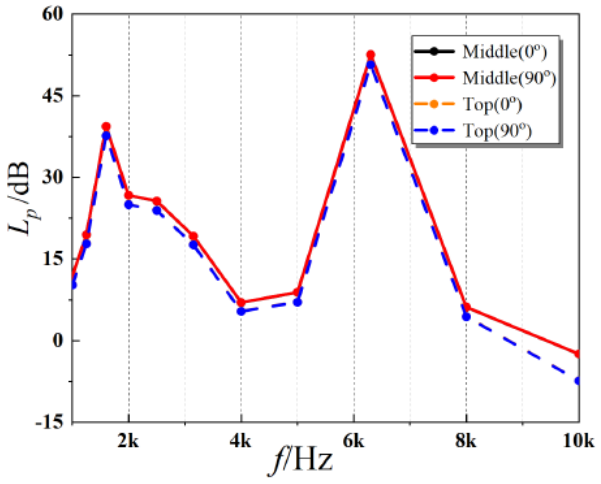

Figure 16: Medium and high frequency sound pressure level curves.

5. CONCLUSION

Our work uses the FEM to calculate the structural vibration response and sound pressure level at low-frequency band and the SEA method to calculate the sound pressure level at the middle and high-frequency bands. These observations are confirmed through comparison with experimental data. The following are the primary conclusions:

1. The vibration response results agree with the experiment in the frequency range of [1,1k] Hz. The sound pressure level results agree with the experiment in the frequency range of [1k,10k] Hz. Analyzing the sound radiation of cylindrical shells with intricate internal structures across the whole frequency range is possible by using the FE-SEA method. The motor's additional mass and the effect of the sound-absorbing equipment on the low-frequency sound wave are the primary sources of experiment error.

2. From the calculation results of the full frequency acoustic radiation, the acoustic radiation results show a large fluctuation in the frequency band of [1,2k] Hz. The sound pressure level peak is near 6k Hz. When the motor operates, the structural acoustic radiation looks like this: The medium and high-frequency bands are comparatively stable. In contrast, the low-frequency bands see significant fluctuations. The primary source of the cylindrical shell's external response and acoustic radiation is its internal excitation. The vibration response and the peak value of sound radiation under excitation force are related to the structure's natural frequency.

3. Compared with the axial position, the level of vibration acceleration on the surface of the water-attached structure has a greater influence on the circumferential position. The circumferential sound pressure level of the water-attached structure becomes more directional with the increased frequency.

In conclusion, it is feasible to use FE-SEA method to analyze the acoustic and vibration characteristics of the structure. The size of the grid needs to be considered in the low-frequency band, and the modal density of the substructure needs to be considered in the medium and high-frequency bands. The calculated frequency ranges of low, medium and high-frequency bands are determined according to the modal density of the substructure. In addition, due to the need to divide more grids in FEM calculation, and with the increase of low-frequency calculation frequency, the grid quality requirements are getting higher and higher, so the calculation range is difficult to involve the full-frequency band, which consumes a lot of time. SEA method does not involve grid division, so the calculation range is easy to involve the whole frequency band, and the computational efficiency is high, but the SEA method focuses on the average energy of the structure, it is difficult to obtain the response of the specific location of the structure. These are the advantages and limitations of both approaches.

ACKNOWLEDGMENTS

This work is supported by the National Natural Science Foundation of China (Grant Nos:12072298; 12172311).

CONFLICT OF INTEREST

The authors declare that they have no conflict of interest.

LIST OF ABBREVIATIONS

a =	acceleration of the experiment and FEM.
a_0 =	the reference value = 10^{-6} $\mathrm{m/s^2}$.
$[B]^T$ =	the boundary matrix of the fluid.
$[C_F]$ =	the damping matrix of the fluid.
$[C_S]$ =	total damping matrix of the structure.
E =	elastic modulus of the structure.
E_i, E_j =	the energy of two subsystems.
$f_{\max}$ =	the upper limit of the frequency calculation range.

$\{F_F\}$ = the acoustic fluid force.

$\{F_S\}$ = the load vector.

h = the thickness of the structure.

$[K_F]$ = the stiffness matrix of the fluid .

$[K_S]$ = total stiffness matrix of the structure.

$L_{\max}$ = the maximum size grid of the model.

$[M_F]$ = the mass matrix of the fluid.

$[M_S]$ = total mass matrix of the structure.

p = pressure of the experiment and FEM.

p_0 = the reference value = 10^{-6} Pa .

$\{p_e\}$ = the node pressure.

$P_{i,in}$ = the input power of the i -th subsystem.

$\{x(t)\}$ = node displacement vector.

$\{\dot{x}(t)\}$ = node velocity vector.

$\{\ddot{x}(t)\}$ = node acceleration vector.

η_{ik} = the coupled loss factor of energy transfer in the i -th subsystem.

η_{ji} = the coupling loss factor of the i -th subsystem transferred to the j -th subsystem.

$\lambda_{\min}$ = the wavelength of bending wave in the medium.

μ = poisson ratio of the structure.

ρ = density of the structure.

$\bar{\rho}_0$ = the density constant of the acoustic fluid.

ω = the center frequency of the analysis band.

FE = Finite element.

FEM = Finite element method.

FE-SEA = Finite element and Statistical energy analysis.

MPC = Multipoint constraint algorithm.

SEA = Statistical energy analysis.

REFERENCES

[1] Leissa A W., Vibration of shells, Scientific and Technical Information Office, National Aeronautics and Space Administration, 1973.

[2] Gan L, Li X, Zhang Z., Free vibration analysis of ring-stiffened cylindrical shells using wave propagation approach, Journal of Sound and Vibration, 2009,326(3-5): 633-646. https://doi.org/10.1016/j.jsv.2009.05.001

[3] Irie T, Yamada G, Muramoto Y., Free vibration of joined conical-cylindrical shells, Journal of Sound and Vibration, 1984,95(1): 31-39. https://doi.org/10.1016/0022-460X(84)90256-6

[4] Ma X, Jin G, Shi S, *et al*., An analytical method for vibration analysis of cylindrical shells coupled with annular plate under general elastic boundary and coupling conditions, Journal of Vibration and Control, 2017,23(2): 305-328. https://doi.org/10.1177/1077546315576301

[5] Polyakov V A, Shlitsa R P, Khitrov V V, *et al*., An applied model for free radial vibrations of a closed spherical sandwich shell, Mechanics of Composite Materials, 2007,43(04): 331-344. https://doi.org/10.1007/s11029-007-0031-1

[6] Hodges C.H., Power J., Woodhouse J., The low frequency vibration of a ribbed cylinder, Part 1: Theory, Journal of Sound and Vibration, 1985,101(02): 219-235. https://doi.org/10.1016/S0022-460X(85)81217-7

[7] Hodges C.H., Power J., Woodhouse J., The low frequency vibration of a ribbed cylinder, Part 2: Observations and interpretation, Journal of Sound and Vibration, 1985,101(02): 237-256. https://doi.org/10.1016/S0022-460X(85)81218-9

[8] Photiadis D M, Houston B H, Williams E G, *et al*., Resonant response of complex shell structures, The Journal of the Acoustical Society of America, 2000,108(3): 1027-1035. https://doi.org/10.1121/1.1286515

[9] Li C, Zhang Z, Yang Q, *et al*., Experiments on the geometrically nonlinear vibration of a thin-walled cylindrical shell with points supported boundary condition, Journal of Sound and Vibration, 2020,473: 115226. https://doi.org/10.1016/j.jsv.2020.115226

[10] Wang Q, Choe K, Shi D, *et al*., Vibration analysis of the coupled doubly-curved revolution shell structures by using Jacobi-Ritz method, International Journal of Mechanical Sciences, 2018,135: 517-531. https://doi.org/10.1016/j.ijmecsci.2017.12.002

[11] Qin Z, Chu F, Zu J., Free vibrations of cylindrical shells with arbitrary boundary conditions: a comparison study, International Journal of Mechanical Sciences, 2017,133: 91-99. https://doi.org/10.1016/j.ijmecsci.2017.08.012

[12] Guo W, Li T, Zhu X, *et al*., Vibration and acoustic radiation of a finite cylindrical shell submerged at finite depth from the free surface, Journal of Sound and Vibration, 2017,393: 338-352. https://doi.org/10.1016/j.jsv.2017.01.003

[13] Aslani P, Sommerfeldt S D, Blotter J D., Analysis of the external radiation from circular cylindrical shells, Journal of Sound and Vibration, 2017,408: 154-167. https://doi.org/10.1016/j.jsv.2017.07.021

[14] Caresta M, Kessissoglou N J., Acoustic signature of a submarine hull under harmonic excitation, Applied acoustics, 2010,71(1): 17-31. https://doi.org/10.1016/j.apacoust.2009.07.008

[15] Wang X, Chen D, Xiong Y, *et al*., Experiment and modeling of vibro-acoustic response of a stiffened submerged cylindrical shell with force and acoustic excitation, Results in Physics, 2018,11: 315-324. https://doi.org/10.1016/j.rinp.2018.09.017

[16] Wang X, Chen D, Xiong Y, *et al*., Simulation and investigations on the vibro-acoustic behavior of cylindrical shells in ice-covered water, Results in Physics, 2019,15: 102764. https://doi.org/10.1016/j.rinp.2019.102764

[17] Wang X, Xu E, Jiang C, *et al*., Vibro-acoustic behavior of double-walled cylindrical shells with general boundary conditions, Ocean Engineering, 2019,192: 106529. https://doi.org/10.1016/j.oceaneng.2019.106529

[18] Wang X Z, Jiang Q Z, Xiong Y P, *et al*., Experimental studies on the vibro-acoustic behavior of a stiffened submerged

conical-cylindrical shell subjected to force and acoustic excitation, Journal of Low Frequency Noise, Vibration and Active Control, 2020,39(2): 280-296. https://doi.org/10.1177/1461348419844648

[19] Jin G, Ma X, Wang W, *et al*., An energy-based formulation for vibro-acoustic analysis of submerged submarine hull structures, Ocean Engineering, 2018,164: 402-413. https://doi.org/10.1016/j.oceaneng.2018.06.057

[20] Yildizdag E, Ardic I T, Kefal A, *et al*., An isogeometric FE-BE method and experimental investigation for the hydroelastic analysis of a horizontal circular cylindrical shell partially filled with fluid, Thin-Walled Structures, 2020,151(17): 106755. https://doi.org/10.1016/j.tws.2020.106755

[21] Gao C, Zhang H, Li H, *et al*., Numerical and experimental investigation of vibro-acoustic characteristics of a submerged stiffened cylindrical shell excited by a mechanical force, Ocean Engineering, 2022,249: 110913. https://doi.org/10.1016/j.oceaneng.2022.110913

[22] Li C, Jian W, Qu Y, *et al*., Numerical and experimental investigation on vibro-acoustic response of a shaft-hull system, Engineering Analysis with Boundary Elements, 2016,71: 129-139. https://doi.org/10.1016/j.enganabound.2016.07.016

[23] Li C, Jian W, Qu Y, *et al*., Vibro-acoustic responses of a coupled propeller-shaft-hull system due to propeller forces, Ocean Engineering, 2019,173: 460-468. https://doi.org/10.1016/j.oceaneng.2018.12.077

[24] Maxit L., Scattering model of a cylindrical shell with internal axisymmetric frames by using the Circumferential Admittance Approach, Applied Acoustics, 2014,80: 10-22. https://doi.org/10.1016/j.apacoust.2014.01.002

[25] Maxit L, Ginoux J M., Prediction of the vibro-acoustic behavior of a submerged shell non periodically stiffened by internal frames, The Journal of the Acoustical Society of America, 2010,128(1): 137-151. https://doi.org/10.1121/1.3436526

[26] Meyer V, Maxit L, Guyader J L, *et al*., Prediction of the vibroacoustic behavior of a submerged shell with non-axisymmetric internal substructures by a condensed transfer function method, Journal of Sound and Vibration, 2016,360: 260-276. https://doi.org/10.1016/j.jsv.2015.09.030

[27] Chen M, Zhang L, Xie K., Vibration analysis of a cylindrical shell coupled with interior structures using a hybrid analytical-numerical approach, Ocean Engineering, 2018,154: 81-93. https://doi.org/10.1016/j.oceaneng.2018.02.006

[28] Ren Y, Qin Y, Pang F, *et al*., Investigation on the flow-induced structure noise of a submerged cone-cylinder-hemisphere combined shell, Ocean Engineering, 2023,270: 113657. https://doi.org/10.1016/j.oceaneng.2023.113657

[29] Gupta P, Parey A., Prediction of sound transmission loss of cylindrical acoustic enclosure using statistical energy analysis and its experimental validation, The Journal of the Acoustical Society of America, 2022,151(1): 544-560. https://doi.org/10.1121/10.0009358

[30] Burroughs C B, Fischer R W, Kern F R., An introduction to statistical energy analysis, The Journal of the Acoustical Society of America, 1997,101(4): 1779-1789. https://doi.org/10.1121/1.418074

[31] Xiang X, Luo H, Li S, *et al*., Characteristics and factors of mode families of axial turbine runner, International Journal of Mechanical Sciences, 2023,251: 108356. https://doi.org/10.1016/j.ijmecsci.2023.108356

[32] Lyon R H, DeJong R G, Heckl M., Theory and application of statistical energy analysis, Boston, USA: Butterworth Heinemann, 1995. https://doi.org/10.1016/C2009-0-26747-X

[33] Yu C, Wang R, Zhang X, *et al*., Experimental and numerical study on underwater radiated noise of AUV, Ocean Engineering, 2020,201: 107111. https://doi.org/10.1016/j.oceaneng.2020.107111

Received on 07-11-2023 Accepted on 15-12-2023 Published on 26-12-2023

DOI: https://doi.org/10.31875/2409-9848.2023.10.15